Fluid dynamical prediction of changed v_1 flow at energies available at the CERN Large Hadron Collider

L. P. Csernai,[1,2,3] V. K. Magas,[4] H. Stöcker,[3] and D. D. Strottman[1,3]

[1]*Institute of Physics and Technology, University of Bergen, Allegaten 55, N-5007 Bergen, Norway*
[2]*MTA-KFKI, Research Institute of Particle and Nuclear Physics, H-1525 Budapest, Hungary*
[3]*Frankfurt Institute for Advanced Studies, Goethe University, D-60438 Frankfurt am Main, Germany*
[4]*Departament d'Estructura i Constituents de la Matèria, Universitat de Barcelona, E-08028 Barcelona, Spain*

Substantial collective flow is observed in collisions between lead nuclei at Large Hadron Collider (LHC) as evidenced by the azimuthal correlations in the transverse momentum distributions of the produced particles. Our calculations indicate that the global v_1-flow, which at RHIC peaked at negative rapidities (named *third flow component* or *antiflow*), now at LHC is going to turn toward forward rapidities (to the same side and direction as the projectile residue). Potentially this can provide a sensitive barometer to estimate the pressure and transport properties of the quark-gluon plasma. Our calculations also take into account the initial state center-of-mass rapidity fluctuations, and demonstrate that these are crucial for v_1 simulations. In order to better study the transverse momentum flow dependence we suggest a new "symmetrized" $v_1^S(p_t)$ function, and we also propose a new method to disentangle global v_1 flow from the contribution generated by the random fluctuations in the initial state. This will enhance the possibilities of studying the collective Global v_1 flow both at the STAR Beam Energy Scan program and at LHC.

I. INTRODUCTION

The first publication from the LHC heavy-ion run presented amazingly strong elliptic flow, exceeding all measurements at lower energies [1]. This indicates strong equilibration and thermalization at these energies in contrast to expectations of increasing transparency. Just six months later ALICE has also measured the v_1 flow [2].

The overall picture indicated by the first v_1 results is very similar for RHIC and ALICE/LHC; namely that v_1 has three physical sources [2,3]: (i) the global collective flow correlated with the reaction plane of the event EP; (ii) the random fluctuation flow of all v_n varieties, where the corresponding symmetry axes (e.g., for v_1 and v_3) have no correlation with the reaction plane EP; instead they are observed with respect to a participant plane PP event by event (EbE) [4,5]. The participant planes are different for the neighboring flow harmonics; (iii) at high momenta or high pseudorapidity, $(1.5 \leqslant |\eta| \leqslant 4)$, there are strong antiflow peaks (in the opposite direction with respect to classical bounce-off). These appear only at RHIC and LHC energies [2,3], and there this is the strongest source of v_1. These high momenta particles are not, and probably cannot be, described by fluid dynamical models. It seems reasonable that they are generated in very early (pre-equilibrium) times of the reaction, and such an emission is anticorrelated with the projectile spectator in the reaction plane due to the shadowing effect of the main reaction volume [6,7]. The hybrid transport AMPT model provided a qualitative match to this v_1 flow component under special assumptions (switching off "sting-melting") [6], what basically means very early (pre-equilibrium?) hadronization and freeze-out in some parts of the reaction volume.

This article discusses the behavior of the first (i), among these flow phenomena, which is the weakest at RHIC and LHC energies. We will also discuss, how to separate the global v_1-flow, from the one produced by random EbE fluctuations of the initial state (ii).

Collective flow is evidenced by the radial flow and, in noncentral collisions, by the asymmetric azimuthal distribution around the beam axis quantified by the functions $v_1(y, p_t)$, $v_2(y, p_t)$, ... in the expansion,

$$\frac{d^3N}{dy\,dp_t\,d\phi} = \frac{1}{2\pi}\frac{d^2N}{dy\,dp_t}[1 + 2v_1\cos(\phi) + 2v_2\cos(2\phi) + \cdots],$$

where y is the rapidity and p_t is the transverse momentum and ϕ is the azimuth angle in the transverse plane with respect to the impact parameter vector, $\vec{b}$.

The observed large $v_2(p_t)$ has important consequences. As the previously observed constituent quark number scaling indicates, the collective flow must have developed in the quark-gluon plasma (QGP) phase, and the flow at the partonic level becomes observable after partons coalesce [8]. Theoretical calculations also indicate that to explain the observed flow, enhanced partonic interaction is needed over perturbative quantum chromodynamics (QCD) predictions [9]. Thus the QGP is strongly interacting. At the same time theoretical estimates and observations also indicate that the QGP is a nearly perfect fluid, with minimal shear viscosity at the phase transition point [10,11].

II. DESCRIPTION OF THE MODEL

The energy-momentum tensor density for a perfect fluid is $T^{\mu\nu} = (e + P)u^\mu u^\nu - Pg^{\mu\nu}$, where P is the local pressure, e is the local energy density, and $u^\mu = \gamma(1, \vec{v})$ is the local flow velocity. We assume the MIT Bag Model Equation of State during the whole calculation.
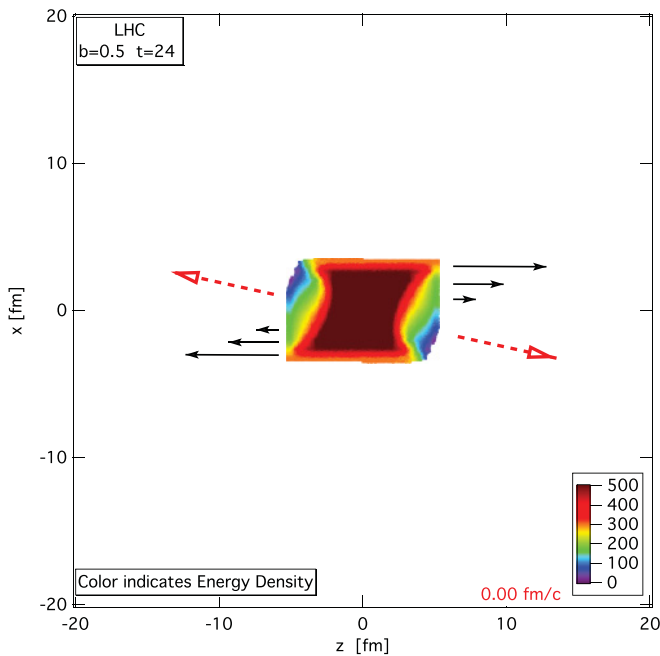
FIG. 1. (Color online) Initial energy density (GeV/fm³) distribution in the reaction plane, (x,y) for a Pb + Pb reaction at 1.38 + 1.38 A TeV collision energy and impact parameter $b = 0.5b_{max}$ at time 4 fm/c after the first touch of the colliding nuclei; this is when the hydro-stage begins. The calculations are performed according to the effective string rope model [12]. This tilted initial state has a flow velocity distribution, qualitatively shown by the arrows. The dashed arrows indicate the direction of the largest pressure gradient at this given moment.

FIG. 2. (Color online) The energy density (GeV/fm³) distribution in the reaction plane, (x,z) for the reaction shown in Fig. 1 at time 12 fm/c after the formation of the hydro initial state. The expected physical FO point is earlier but this post-FO configuration illustrates the flow pattern.

A fluid dynamical (FD) description of the nuclear matter is considered here for Pb + Pb collisions at 1.38 + 1.38 A TeV. The matter expands until it reaches freeze-out (FO). The FD description does not constrain the FO: an external condition, for example, a fixed FO temperature, is needed. The FD model we use [13–15] can run well beyond the FO, so the location of physical FO can be selected afterward as a space-time hypersurface.

The (3+1)-dimensional, FD model [13–15] uses the Particle in Cell (PIC) method adapted to ultrarelativistic heavy-ion collisions. The numerical dissipation of the method was analyzed recently in Ref. [16]. In this method, marker particles, corresponding to fixed baryon charge, move in an Eulerian grid. The calculation, describing the reaction, starts from an analytic initial state model [12], based on longitudinally expanding strings of the color-magnetic field. The produced initial state, shown in Fig. 1, is tilted, and, thus, the direction of the largest pressure gradient is pointing in the "antiflow" direction, what resulted in antiflow peaks in simulations for RHIC and SPS [17,18]. However, one should not forget that this initial state also has a flow velocity distribution, which tends to further rotate it; that is, effectively it has a large initial "angular momentum" that will change the direction of the strongest pressure gradient with time.

Figure 2 shows the energy density distribution in the reaction plane later. One may notice that the final state is strongly rotated with respect to the initial one, due to the large
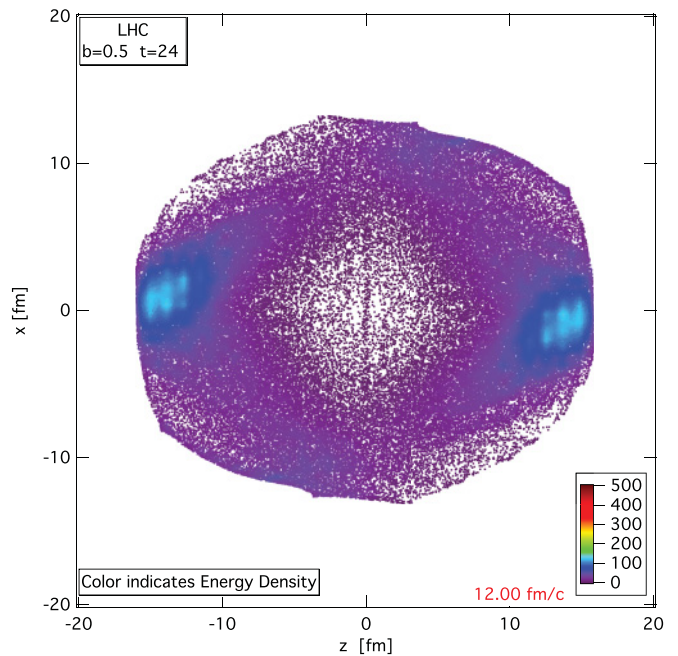
initial "angular momentum," and the direction of the strongest transverse expansion points to $\Theta = 75/255°$. Thus, the upward moving matter is moving now forward and the downward moving matter backward, in contrast to what happens at RHIC and SPS energies [14].

The fluid cells in the presented calculations were (0.438 fm)³ for peripheral collisions, $b = 0.5 - 0.7b_{max}$. While initially we had 2500–5400 fluid cells containing matter, this increased over 100 000 by the end of calculation. The higher energy at LHC results in a more explosive expansion, which leads to an explosion shell with decreasing central density.

In a simplest approach we assume a constant time FO hypersurface. Comparing measured multiplicity b dependence at LHC with our FD multiplicity, we have chosen $t_{FO} = 8$ fm/c after the formation of the hydro initial state. The transition from pre-FO QGP to post-FO ideal massless pion Jüttner gas is calculated according to the method described in Ref. [19], satisfying the conservation laws. In this way for each fluid cell i, we obtain a flow velocity $\vec{v}^i = (\vec{v}_t{}^i, v_z^i)$ of the gas and its temperature T^i.

Using the Cooper-Frye FO formula we obtain

$$v_n(y, p_t) = \frac{\sum_i^{cells} \int_0^{2\pi} d\phi \; f^i(y, \vec{p}_t) \; \cos n\phi}{\sum_i^{cells} \int_0^{2\pi} d\phi \; f^i(y, \vec{p}_t)}, \quad (1)$$

where $f^i(y, \vec{p}_t)$ is the normalized momentum distribution for cell i; the angle ϕ is taken with respect to the reaction plane.

Then,

$$v_n(y) = \frac{\sum_i^{\text{cells}} J_n(y, \vec{v}^{\,i}, T^i) \cos(n\phi_0^i)}{\sum_i^{\text{cells}} J_0(y, \vec{v}^{\,i}, T^i)}, \quad (2)$$

$$v_n(p_t) = \frac{\sum_i^{\text{cells}} B(\vec{v}^{\,i}, T^i, p_t) I_n(\gamma^i v_t^i p_t/T^i) \cos(n\phi_0^i)}{\sum_i^{\text{cells}} B(\vec{v}^{\,i}, T^i, p_t) I_0(\gamma^i v_t^i p_t/T^i)},$$

$$J_n(y, \vec{v}^{\,i}, T^i) = \int_0^\infty dp_t\, p_t^2 I_n(\gamma_t^i \tilde{v}_t^i p_t/T^i) e^{-\gamma_t^i p_t \cosh(y-y_0^i)/T^i},$$

$$B(\vec{v}, T, p_t) = e^{-\gamma p_t/T} \frac{1}{1-v_z^2} \left(v_z \frac{T}{\gamma} - p_t|v_z| \right) \quad (3)$$
$$+ \frac{p_t}{\sqrt{1-v_z^2}} K_1\left(\gamma p_t \sqrt{1-v_z^2}/T, \gamma p_t/T\right),$$

where y_0^i is the flow rapidity and ϕ_0^i is the azimuthal angle of the flow velocity in the transverse plane of the given cell i. In Eq. (2) we have rewritten flow 4-velocity in the following way: $u_i^\mu = \gamma_t^i(\cosh y_0^i, \sinh y_0^i, \vec{\tilde{v}}_t^i)$, with $\vec{\tilde{v}}_t^i = \vec{v}_t^i/\sqrt{1-(v_z^i)^2}$, $\gamma_t^i = 1/\sqrt{1-(\tilde{v}_t^i)^2}$. I_n is a Bessel function, and $K_1(a, b) = \frac{1}{a}\int_b^\infty dx \sqrt{x^2-a^2} e^{-x}$ is a modified Bessel function of the second kind.

III. RESULTS: p_t DEPENDENCE OF THE FLOW

The calculated $v_2(p_t)$ distributions are similar to the experimental trends. For illustration one calculated $v_2(p_t)$ distribution is presented in Fig. 3. The solid curve, calculated according to Eq. (3), is slightly below the experimental data. This can be attributed to the integral over the whole rapidity range, while the experiment is only for $|\eta| < 0.8$, and to the initial state fluctuations, as discussed below.

As v_1 is an antisymmetric function of y, the y-integrated $v_1(p_t)$ value must vanish. In our calculation this is realized
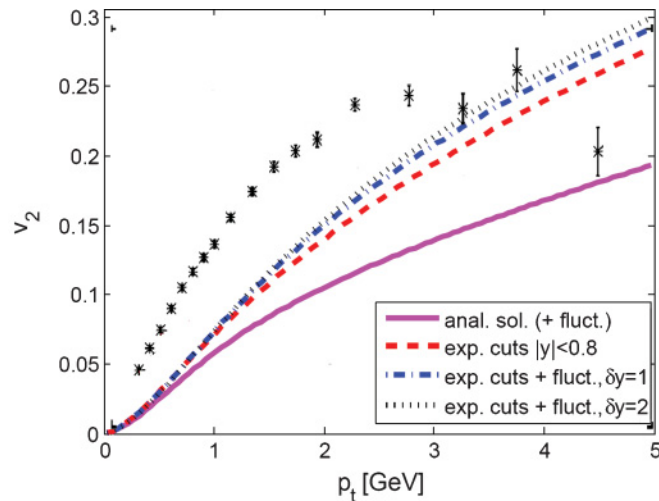

FIG. 3. (Color online) The v_2 parameter calculated for ideal massless pion Juttner gas, versus the transverse momentum, p_t for $b = 0.7 b_{\max}$, at $t = 8$ fm/c FO time. The magnitude of v_2 is comparable to the observed v_2 at 40%–50% centrality (black stars). See text for more explanation of different curves.
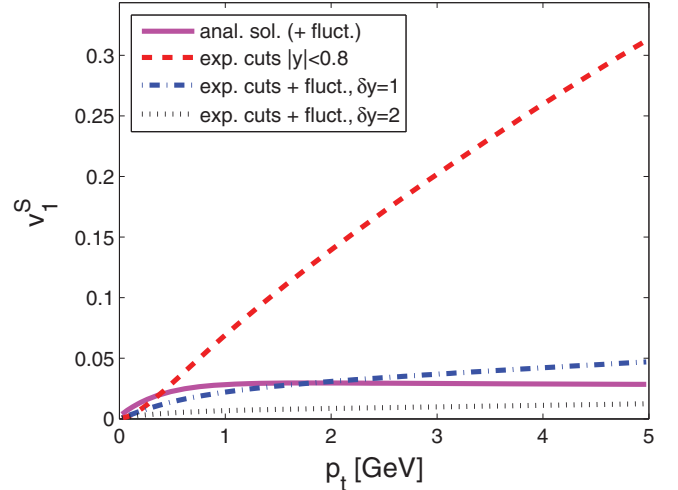

FIG. 4. (Color online) The v_1^S flow parameter calculated according to Eq. (5) for ideal massless pion Juttner gas, versus the transverse momentum, p_t for $b = 0.7 b_{\max}$, at $t = 8$ fm/c FO time. See text for explanation of different curves.

to an accuracy better than 10^{-16}. However, considering this obvious asymmetry, we propose to construct a symmetrized function v_1^S reversing the $\vec{p}_t$ direction of backward going $(y < 0)$ particles:

$$v_1^S(y, p_t) = \frac{\sum_i^{\text{cells}} \int_0^{2\pi} d\phi\, f^i(y, \text{sgn}(y) \cdot \vec{p}_t)\, \cos\phi}{\sum_i^{\text{cells}} \int_0^{2\pi} d\phi\, f^i(y, \text{sgn}(y) \cdot \vec{p}_t)}, \quad (4)$$

where $\text{sgn}(y)$ extracts the sign of rapidity. The idea stems from Danielewicz and Odyniecz [20]. In this way we get a nonvanishing $v_1^S(p_t)$ function, which will be also much less sensitive to the initial state fluctuations.

$$v_1^S(p_t) = \frac{\sum_i^{\text{cells}} 2D(\vec{v}^{\,i}, T^i, p_t) I_1(\gamma^i v_t^i p_t/T^i) \cos(\phi_0^i)}{\sum_i^{\text{cells}} B(\vec{v}^{\,i}, T^i, p_t) I_0(\gamma^i v_t^i p_t/T^i)}, \quad (5)$$

where $D(\vec{v}, T, p_t) = e^{-\gamma p_t/T} \frac{v_z}{1-v_z^2} \frac{T}{\gamma}$. The $v_1^S(p_t)$ parameter calculated in this way is shown in Fig. 4 (solid line).

The ALICE team has made a detailed symmetry analysis of the low rapidity component in the acceptance range of the ALICE TPC [2]. They introduced new quantities,

$$v_1^{\text{even/odd}}(\eta, p_t) = [v_1(\eta, p_t) \pm v_1(-\eta, p_t)]/2, \quad (6)$$

$$v_1(\eta, p_t) = v_1^{\text{even}}(\eta, p_t) + v_1^{\text{odd}}(\eta, p_t). \quad (7)$$

If we have a global mirror asymmetric (MA) v_1 flow only, as in our hydrodynamical simulations, then the *even* component vanishes:

$$v_1^{\text{even}}(\eta, p_t) = 0, \quad v_1^{\text{odd}}(\eta, p_t) = v_1(\eta, p_t). \quad (8)$$

A nonvanishing $v_1^{\text{even}}(\eta, p_t)$ can only come from the mirror symmetric (MS) part of random fluctuation flow.

Furthermore, if we will integrate over (pseudo-) rapidity, then, as it was discussed above, the global $v_1(p_t)$ flow, correlated with the reaction plane of the event, is exactly zero. Thus, nonzero $v_1^{\text{even}}(p_t)$ and $v_1^{\text{odd}}(p_t)$ can only come from the random fluctuation in the initial state. Without other assumption, we should not make any difference for MS and

MA fluctuations, and thus these two components should be (approximately) equal: $v_1^{\text{even}}(p_t) = v_1^{\text{odd}}(p_t)$. The preliminary ALICE results [2] clearly confirm the simple logical sequence. So, we can conclude that $v_1^{\text{even}}(p_t) = v_1^{\text{odd}}(p_t)$ observed by ALICE collaboration come from the second v_1 flow source (ii), and cannot tell us anything about global v_1 flow (i).

However, we can gain information about the p_t dependence of the global directed flow, if we repeat the same analysis (i.e., separation into *even* and *odd* components) for the $v_1^S(y, p_t)$ function, introduced above [Eq. (4)]. Indeed, we obtain

$$v_1^{S,\text{odd}}(p_t) = v_{1,\text{fluct.}}^S(p_t), \tag{9}$$

$$v_1^{S,\text{even}}(p_t) = v_1^S(p_t) + v_{1,\text{fluct.}}^S(p_t), \tag{10}$$

where $v_{1,\text{fluct.}}^S(p_t)$ is a contribution to the v_1^S function from the initial state fluctuations, which is approximately equal for both components, as discussed above. Thus, in this case we can separate the contributions from the (i) and (ii) sources:

$$v_{1,\text{fluct.}}^S(p_t) = v_1^{S,\text{odd}}(p_t), \tag{11}$$

$$v_1^S(p_t) = v_1^{S,\text{even}}(p_t) - v_1^{S,\text{odd}}(p_t). \tag{12}$$

IV. RESULTS: RAPIDITY DEPENDENCE OF THE FLOW

The $v_1(y)$ dependence is shown in Fig. 5 [solid line is the analytic solution; Eq. (2)]. As we can see the v_1 is relatively large in the experimental rapidity range $|y| \leqslant 0.8$, reaching a peak of 26% at $y = \pm 0.5$. The most important change with respect to the similar simulations for RHIC [18] is that the v_1 now peaks in "forward" direction (i.e., the positive peak appears now at positive rapidity).

Qualitatively our results agree with the simulations performed in a microscopic transport model, namely the quark
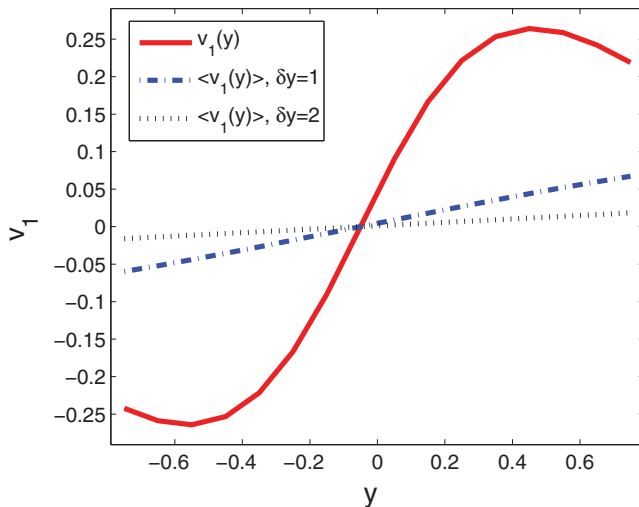

FIG. 5. (Color online) The v_1 parameter calculated for ideal massless pion Juttner gas, versus the rapidity y for $b = 0.7b_{\text{max}}$, at $t = 8$ fm/c FO time. Full curve presents semianalytical calculations according to Eq. (2); the v_1 peak appears at positive rapidity, in contrast to lower energy calculations and measurements. The dash-dotted and dotted curves present v_1 calculated taking into account initial c.m. rapidity fluctuations.

gluon string model [7], where $v_1(\eta)$ in "forward" direction was obtained. However, the authors of [7] have not found the reason for such a behavior, and have qualitatively attributed it to the different viscosities in the region with $|\eta| < 3$ and at higher pseudorapidities.

At lower energies in the same FD model calculations we obtained the v_1 peaking in the "backward" direction (*third flow component*) [17,18], of a magnitude of 5% and 2%–3% for 158 and 65 + 65 A·GeV energy, respectively. The position of the peaks also moved from $|y| \approx 1.5$ to $|y| \approx 0.5$ with energy increasing from SPS to RHIC. Experimentally the third-flow component was indeed measured at these energies [3,17,21], although the peak values were smaller. Especially at the RHIC energies [3], where the highest values were $v_1 \approx 0.6$ % and 0.2% for for 62.4 + 62.4 and 200 A·GeV energy, respectively. The peaks appeared at $|y| \approx 1$ around the far end of the acceptance of the central TPC. Thus, at RHIC the v_1 magnitude was about 5 times smaller than the FD prediction. Also, the move toward the more central rapidities was weaker in the experiment than in FD calculations.

The reason for such a disagreement is the effect of initial state center of mass (c.m.) rapidity fluctuations, which may be decisive in the case of v_1 because of the sharp change around $y = 0$.

V. INITIAL STATE C.M. RAPIDITY FLUCTUATIONS

One has to take into account that the c.m. rapidity is not exactly the same for all collisions because of random fluctuations in the initial state, where the numbers of participant nucleons from projectile and target may not be exactly the same. This leads to considerable $y_{\text{c.m.}}$ fluctuations at large impact parameters, where the flow asymmetry is the strongest, whereas the total number of participants is the smallest. Although several initial state models generate EbE fluctuating initial states (see, e.g., [22]), longitudinal fluctuations are not analyzed up to now, neither theoretically nor experimentally in detail. A high acceptance experiment could provide a good estimate for the EbE initial state rapidity, $y_{\text{c.m.}}$ [23], which is a conserved quantity (i.e., it cannot be changed by the system expansion, hadronization, or freeze-out).

To analyze the consequences of these fluctuations, we assumed a Gaussian $y_{\text{c.m.}}$ distribution, centered at $y_{\text{c.m.}} = 0$, with variance $\delta y = 1, 2$.

Results can be seen in Fig. 5: dash-dotted and dotted lines. As expected the initial state fluctuations strongly reduce $v_1(y)$ at central rapidities. The resulting v_1 is still large enough to demonstrate the "rotation effect" discussed above, however, being of the order of 1% it can be easily masked by the directed flow generated by the random fluctuations in the initial state.

The first preliminary results from LHC [2] show $v_1(\eta)$ at midrapidity of the order of 0.1% or less, in antiflow direction. Taking into account the error bars, the observed directed flow at LHC is very little, practically compared with 0. This might be a result of a compensation of the $v_1(\eta)$ in "backward" (antiflow) direction, coming from the random fluctuations in the initial state [5,22], with the global directed flow in the "forward" direction, as predicted by our simulations.
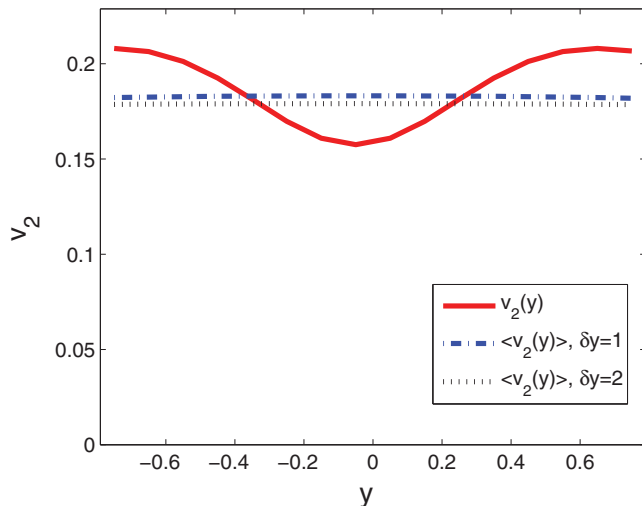
FIG. 6. (Color online) The v_2 parameter calculated for ideal massless pion Juttner gas, versus the rapidity y for $b = 0.7b_{\mathrm{max}}$, at $t = 8$ fm/c FO time. Full curve presents semianalytical calculations according to Eq. (2); dash-dotted and dotted curves present v_2 calculated taking into account initial c.m. rapidity fluctuations.

It is interesting to study the effects of the initial c.m. rapidity fluctuations on other observables. Figure 6 shows the elliptic flow as a function of rapidity. Fluctuations make the $v_2(y)$ peaks wider, but the magnitude is hardly reduced. Thus, we predict a plateaulike shape of the elliptic flow distribution.

The c.m. rapidity fluctuations have, in principle, no effect on the y-integrated $v_2(p_t)$ and $v_1^S(p_t)$ [therefore the solid line in Figs. 3 and 4 are marked as "analytical solution (+ fluctuations)"]. However, in the realistic simulations, we should not integrate over y from $-\infty$ to $+\infty$, but only over the measured rapidity range (i.e., $-0.8 \leqslant y \leqslant 0.8$). Such a "limited range" effect is dramatic for $v_1^S(p_t)$ which can be reduced to less than 1% (see the dashed and dotted lines in

Fig. 4). The $v_2(p_t)$ dependence is weakly affected (Fig. 3, dashed line).

Interestingly, the initial $y_{\mathrm{c.m.}}$ fluctuations lead to some increase of the elliptic flow, $v_2(p_t)$, putting it in a reasonable agreement with the ALICE data [1] (see Fig. 3; please note that no fine-tuning was done). At the same time $y_{\mathrm{c.m.}}$ fluctuations strongly reduce $v_1^S(p_t)$ (see Fig. 4).

VI. SUMMARY

Our FD simulations of the LHC heavy-ion collisions suggest that collective directed $v_1(y)$ flow and newly introduced $v_1^S(p_t)$ function can and should be measured [23], although these are strongly suppressed due to initial state $y_{\mathrm{c.m.}}$ fluctuations (see Figs. 4 and 6). For the first time in hydrodynamical calculations we see that the v_1 global flow can change the direction to "forward" in contrast to what happened at lower energies. This is a result of our tilted and moving initial state [12], in which the effective "angular momentum" from the increasing beam momentum is superseding the expansion driven by the pressure. We have also proposed a new method to distinguish contributions to $v_1(p_t)$ from global flow (i) and from random fluctuations in the initial state (ii). The method is based on $v_1^S(p_t)$ function, introduced by us in this work, and consists in analyzing its even and odd components according to Eq. (12).

[1] K. Aamodt *et al.* (The ALICE Collaboration), Phys. Rev. Lett. **105**, 252302 (2010).

[2] R. Snellings, Presentation at the 22nd International Conference on Ultra-Relativistic Nucleus-Nucleus Collisions (Quark Matter 2011), Annecy, France, May 23–28, 2011; I. Shelyuzenkov, *ibid.*; G. Eyyubova, *ibid.*

[3] B. I. Abelev *et al.* (STAR Collaboration), Phys. Rev. Lett. **101**, 252301 (2008).

[4] N. Borghini, P. M. Dinh, and J. Y. Ollitrault, Phys. Rev. C **64**, 054901 (2001); J. Schukraft, Presentation at the 22nd International Conference on Ultra-Relativistic Nucleus-Nucleus Collisions (Quark Matter 2011), Annecy, France, May 23–28, 2011.

[5] B. Schenke, Presentation at the 22nd International Conference on Ultra-Relativistic Nucleus-Nucleus Collisions (Quark Matter 2011), Annecy, France, May 23–28, 2011.

[6] L. W. Chen and C. M. Ko, J. Phys. G **31**, S49 (2005).

[7] J. Bleibel, G. Burau, and C. Fuchs, Phys. Lett. B **659**, 520 (2008).

[8] D. Molnár and S. A. Voloshin, Phys. Rev. Lett. **91**, 092301 (2003); V. Greco, C.-M. Ko, and P. Lévai, Phys. Rev. C **68**, 034904 (2003); R. J. Fries, B. Müller, C. Nonaka, and S. A. Bass, *ibid.* **68**, 044902 (2003).

[9] D. Molnár and M. Gyulassy, Nucl. Phys. A **697**, 495 (2002); **703**, 893(E) (2002).

[10] P. K. Kovtun, D. T. Son, and A. O. Starinets, Phys. Rev. Lett. **94**, 111601 (2005).

[11] L. P. Csernai, J. I. Kapusta, and L. D. McLerran, Phys. Rev. Lett. **97**, 152303 (2006).

[12] V. K. Magas, L. P. Csernai, and D. D. Strottman, Phys. Rev. C **64**, 014901 (2001); Nucl. Phys. A **712**, 167 (2002).

[13] L. P. Csernai, Y. Cheng, V. K. Magas, I. N. Mishustin, and D. Strottman, Nucl. Phys. A **834**, 261c (2010).

[14] L. P. Csernai *et al.*, J. Phys. G **36**, 064032 (2009).

[15] L. Bravina, L. P. Csernai, P. Lévai, and D. Strottman, Phys. Rev. C **50**, 2161 (1994).

[16] Sz. Horvat, V. K. Magas, D. D. Strottman, and L. P. Csernai, Phys. Lett. B **692**, 277 (2010).

[17] L. P. Csernai and D. Röhrich, Phys. Lett. B **458**, 454 (1999).

[18] B. Bäuchle *et al*., J. Phys. G **34**, s1077 (2007).

[19] Y. Cheng, L. P. Csernai, V. K. Magas, B. R. Schlei, and D. Strottman, Phys. Rev. C **81**, 064910 (2010).

[20] P. Danielevicz and G. Odyniecz, Phys. Lett. B **157**, 146 (1985).

[21] G. Wang *et al*. (STAR Collaboration), J. Phys. G **34**, s1093 (2007).

[22] F. G. Gardim, F. Grassi, Y. Hama, M. Luzum, and J. Y. Ollitrault, Phys. Rev. C **83**, 064901 (2011).

[23] D. Röhrich (ALICE Collaboration), private communication.